International Journal of Minerals, Metallurgy and Materials
Volume 28, Number 2, February 2021, Page 249
https://doi.org/10.1007/s12613-020-2167-0

Effect of nanosized NbC precipitates on hydrogen-induced cracking of high-strength low-alloy steel

En-dian Fan[1)], *Shi-qi Zhang*[1,2)], *Dong-han Xie*[1)], *Qi-yue Zhao*[1)], *Xiao-gang Li*[1,3)], *and Yun-hua Huang*[1)]

1) Institution for Advanced Materials and Technology, University of Science and Technology Beijing, Beijing 100083, China
2) Key Laboratory of Advanced Materials (MOE), School of Materials Science and Engineering, Tsinghua University, Beijing 100084, China
3) Ningbo Institute of Material Technology & Engineering, Chinese Academy of Sciences, Ningbo 315201, China
(Received: 27 December 2019; revised: 7 August 2020; accepted: 10 August 2020)

Abstract: We investigated the effect of nanosized NbC precipitates on hydrogen-induced cracking (HIC) of high-strength low-alloy steel by conducting slow-strain-rate tensile tests (SSRT) and performing continuous hydrogen charging and fracture analysis. The results reveal that the HIC resistance of Nb-bearing steel is obviously superior to that of Nb-free steel, with the fractured Nb-bearing steel in the SSRT exhibiting a smaller ratio of elongation reduction (I_δ). However, as the hydrogen traps induced by NbC precipitates approach hydrogen saturation, the effect of the precipitates on the HIC resistance attenuate. We speculate that the highly dispersed nanosized NbC precipitates act as irreversible hydrogen traps that hinder the accumulation of hydrogen at potential crack nucleation sites. In addition, much like Nb-free steel, the Nb-bearing steel exhibits both H-solution strengthening and the resistance to HIC.

Keywords: nanosized NbC precipitates; high-strength low-alloy steel; hydrogen-induced cracking; slow-strain-rate tensile, hydrogen charging

1. Introduction

With the growing development and utilization of marine resources, more high-strength low-alloy (HSLA) steels are being utilized in marine platforms and submarine petroleum transportation. With an increase in the strength of steel, the risk of hydrogen-induced cracking (HIC) increases significantly in the harsh marine environment, which has restricted the development of offshore engineering [1–5]. It has been claimed that precipitation expedites nucleation and propagation during HIC [6–8], but other researchers have reported that dispersed and nanosized precipitates are beneficial to HIC resistance [9–12]. Thus, it is evident that the effect of precipitates on HIC susceptibility is not yet fully understood.

In recent years, research has focused on improving the HIC resistance of high-strength steel by the use of microalloy elements (e.g., Nb, V, and Ti) [11–16]. Nagao *et al*. [13] reported that nanosized precipitates of Ti–Mo carbide can improve the HIC resistance of high-strength tempered lath martensitic steel because a great number of these precipitates act as hydrogen traps. Zhang *et al.* [11,17] investigated the effect of Nb on HIC susceptibility in HSLA steel and reported that the HIC resistance of the steel was significantly improved by Nb microalloying, in which NbC precipitates act as irreversible traps that pin hydrogen atoms, causing them to be distributed uniformly throughout the matrix. Other researchers have focused on the strengthening and toughening of microalloy elements and their precipitates. The high strength and toughness of Nb, V, and/or Ti microalloyed steels are reported to be primarily due to grain refinement and precipitation strengthening [18–20]. The mechanism of grain refinement is related to the microalloy elements that generally form carbide or nitride characterized by a high level of hardness and a high melting point. These compounds play a very important role in restraining the growth of austenite grains and inhibiting austenite recrystallization [21]. In addition, studies have revealed that non-metallic inclusions and precipitation phases are the dominant factors affecting hydrogen traps and hydrogen damage [17,22–24], although the existence of a direct correlation between nano-precipitates and the HIC of HSLA steels remains uncertain.

In this work, we investigated the microstructure, mechanics, and fracture behavior of HSLA steels. We conducted

Corresponding author: Yun-hua Huang E-mail: huangyh@mater.ustb.edu.cn

slow-strain-rate tensile tests (SSRT) and a fracture analysis to determine the effects of NbC precipitates on the HIC behavior of the steels, and we studied the mechanism of HIC resistance. The results of this study will facilitate the development of HSLA steels that contain the microalloy element Nb.

2. Experimental

2.1. Materials

The steel used in this study, which was produced in our laboratory, was an HSLA steel grade API X80 used in pipeline manufacturing. Table 1 shows the chemical composition of this steel, as determined using direct-reading emission spectrometry. The labels Nb-bearing and Nb-free correspond to steels with Nb contents of 0.055wt% and 0wt%, respectively. The two types of X80 plate samples were hot-rolled at about 1200°C, and then air-cooled to 830°C for the second rolling. This cooling time is conducive to the precipitation of NbC particles. There are two steps in the cooling process: water quenching to 430–470°C immediately after the final rolling to obtain bainite, and then cooling to room temperature in air.

Table 1. Chemical composition of the investigated steels wt%

Steel	C	Si	Mn	P	S	Nb	Ti	Mo	Ni	Cu
Nb-bearing	0.060	0.27	1.84	0.004	0.005	0.055	0.015	0.25	0.26	0.26
Nb-free	0.058	0.28	1.85	0.004	0.006	—	0.016	0.26	0.26	0.26

2.2. Procedures

Optical microscopy (Reichert-Jung Polyvar MET) and transmission electron microscopy (TEM, FEI Tecn G2 F20) with a voltage of 100 kV were used to observe the microstructure and nanosized NbC precipitates of the samples. In addition, scanning electron microscopy (FEI Quant250) was used to examine micrographs of the top views of typical fracture surfaces.

The samples were ground using SiC sandpaper with 240–2000 grit, cleaned with distilled water, and then dried with ethanol. After hydrogen pre-charging of the samples for 3 h in a pressure cell filled with a 0.2 $mol \cdot L^{-1}$ NaOH and 0.25 $g \cdot L^{-1}$ CH_4N_2S solution, the SSRT were performed at 25°C using a WDML 30 kN SSRT system (Fig. 1) at a strain rate of 1×10^{-6} s^{-1} in the same solution. The SSRT were performed with continuous hydrogen charging at respective current densities of 0, 2, 5, and 10 $mA \cdot cm^{-2}$ to evaluate the HIC resistance. The samples for the SSRT and hydrogen-charging tests were cut from the X80 plates according to the GB/T15790 standard, with the dimensions shown in Fig. 2.

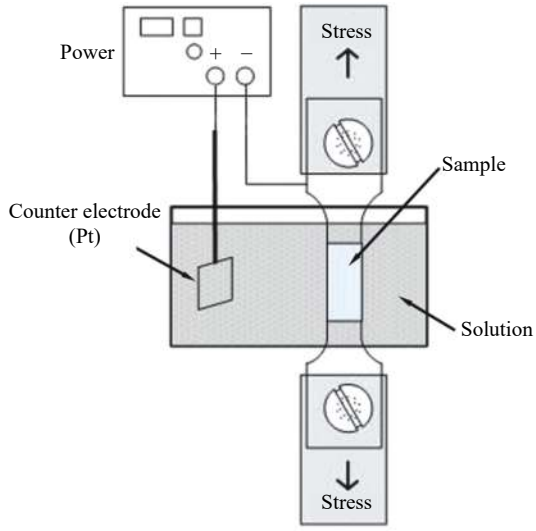

Fig. 1. Schematic of the SSRT apparatus.

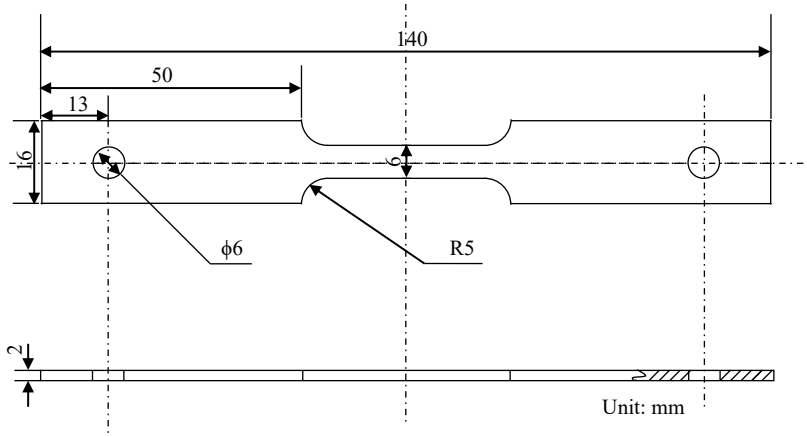

Fig. 2. Shape and size of the tensile samples.

3. Results and discussion

3.1. Microstructure

The typical microstructure of X80 steel is granular bainite, lath bainite, or lath martensite [10,16,25]. Figs. 3(a) and 3(b) show optical micrographs of the microstructures of the Nb-bearing and Nb-free samples, respectively. Compared with the Nb-free sample, the grain size of the Nb-bearing sample is smaller. We compared the grain sizes and morphologies of the Nb-bearing and Nb-free samples using electron backscattered diffraction (EBSD), as shown in Fig. 4. From the inverse pole figures, we can see that the Nb-bearing sample was more regular polygonal granular bainite grains, whereas the Nb-free sample had larger and uneven sized granular bainite grains, and was mixed with some lath bainite. These differences are attributed to grain refinement, which is because that NbC precipitates effectively inhibit the growth of austenite grains, and the dissolved Nb effectively halts recrystallization, as demonstrated in previous studies [26–27]. The statistical results show that the average grain size of the Nb-bearing sample was 8.9 μm, whereas that of the Nb-free sample was 10.5 μm.

Next, we examined the nanosized precipitates in the experimental steel by TEM, as shown in Fig. 5(a). A large number of precipitates with an average size much less than 10 nm are uniformly distributed throughout the matrix, and form coherent interfaces with the bcc-Fe matrix. Using high-resolution analysis, the precipitates were indexed as NbC, as shown

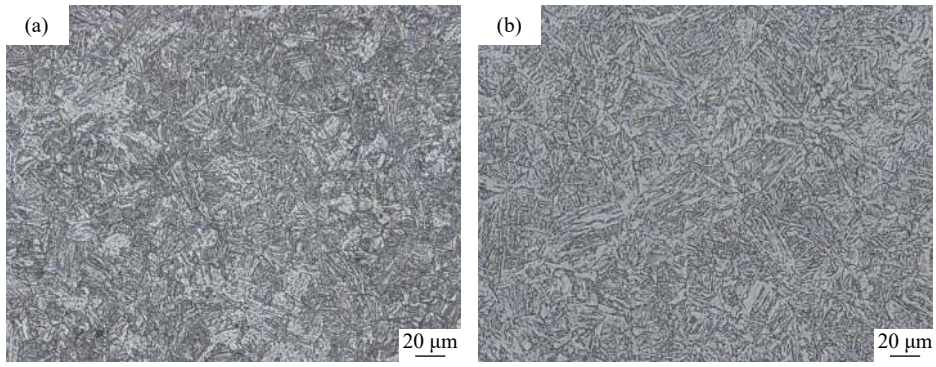

Fig. 3. Microstructures of steel samples (4vol% nital solution): (a) Nb-bearing; (b) Nb-free.

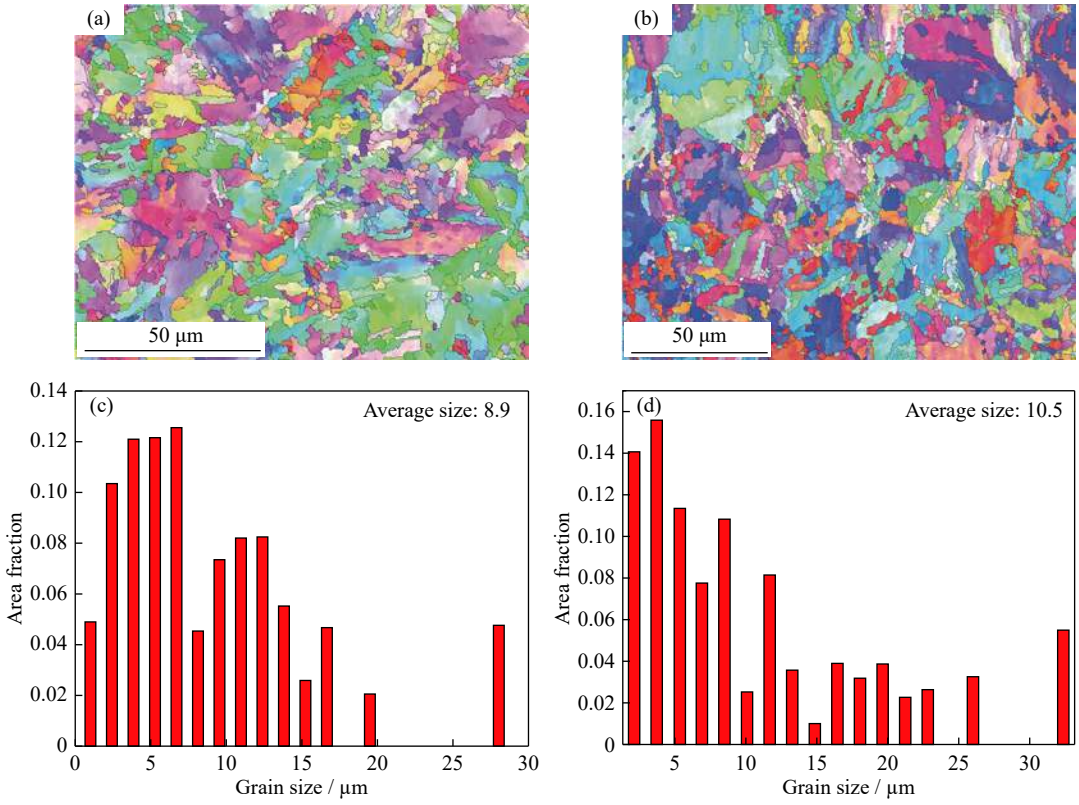

Fig. 4. Inverse pole figures and grain sizes of the HSLA steel samples obtained by EBSD: (a, c) Nb-bearing; (b, d) Nb-free.

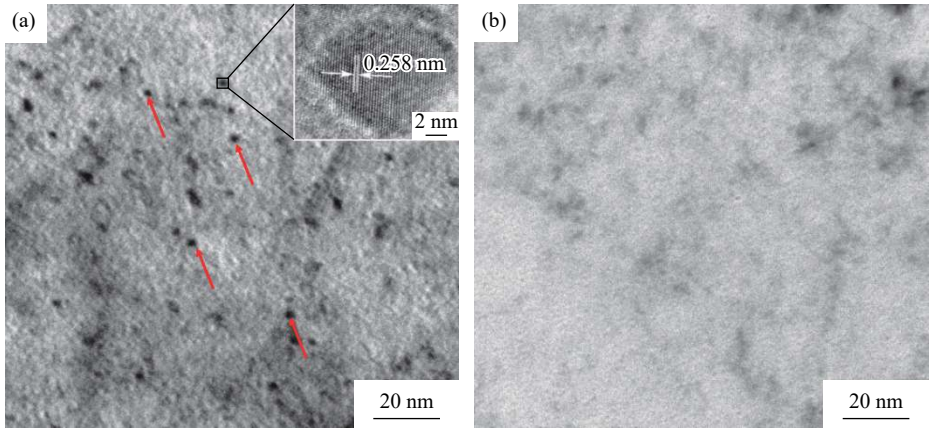

Fig. 5. TEM morphologies of samples: (a) Nb-bearing and the high-resolution TEM image of a precipitate embedded in right-hand side; (b) Nb-free.

in the inset of Fig. 5(a). In contrast, no precipitates appeared in the Nb-free sample, as shown in Fig. 5(b).

3.2. Mechanical properties

The stress–strain curves of samples with different hydrogen-charging current densities (0, 2, 5, and 10 mA·cm^{-2}, respectively) are shown in Fig. 6, and the corresponding curves of tensile strength (σ_b) and elongation (δ) versus the charging current density are shown in Fig. 7.

The strength of the Nb-bearing samples was obviously higher than that of the Nb-free samples, which is due to the precipitation strengthening and fine-grain strengthening of the NbC. The tensile strength first increased and then decreased with an increase in the hydrogen-charging current density (Fig. 7(a)). According to the principle of cathodic hydrogen charging, the hydrogen evolution reaction on the

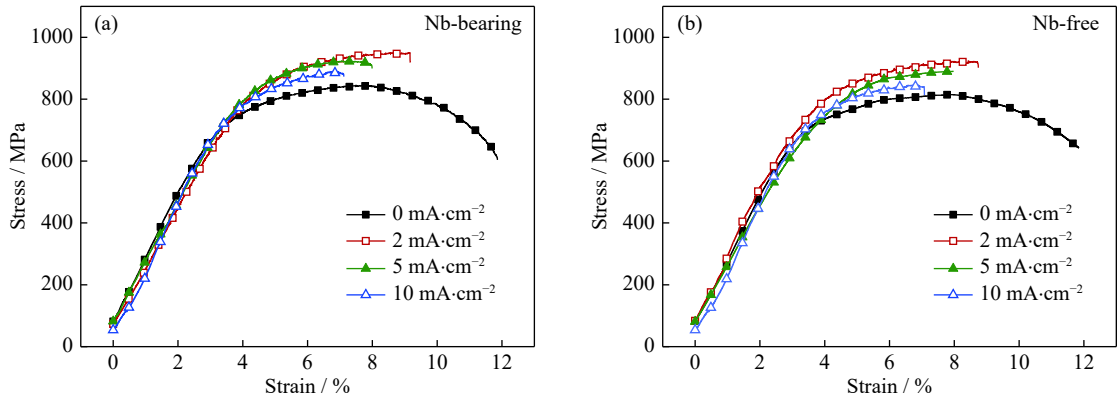

Fig. 6. Stress–strain curves of the samples at different current densities: (a) Nb-bearing; (b) Nb-free.

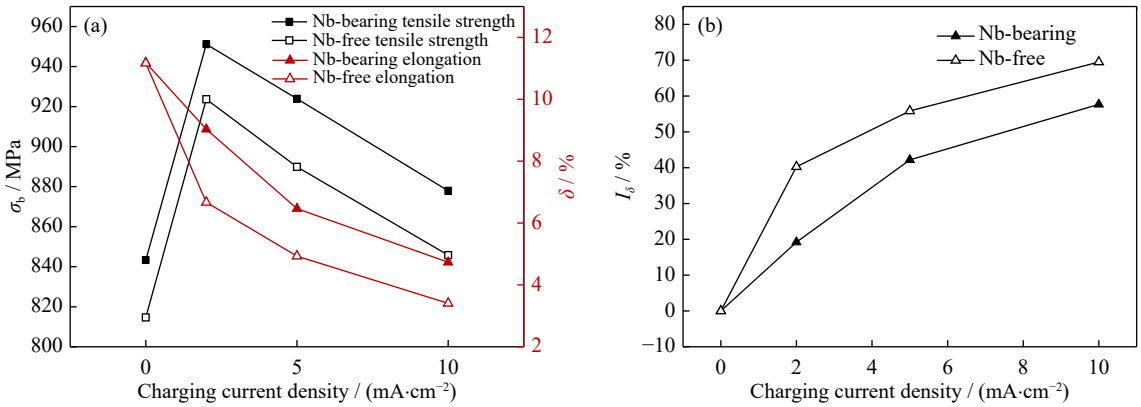

Fig. 7. Curves of tensile strength (σ_b), elongation (δ), and reduction ratio of elongation (I_δ) for the Nb-bearing and Nb-free samples vs. charging current density: (a) tensile strength and elongation; (b) reduction ratio of elongation.

cathode sample surface increases with an increase in the current density at constant temperature [28–29]. As such, more hydrogen atoms are adsorbed and diffused into the sample matrix as the current density increases, which results in the higher hydrogen content [30]. Therefore, when the hydrogen-charging current density was lower than 2 mA·cm^{-2}, few hydrogen atoms were brought into the samples, and the tensile strength increased with an increase in the current density. The reason for this is that hydrogen atoms mainly function as solution-strengthening elements when the hydrogen content is lower than a critical hydrogen damage value [31–32]. When the current density was higher than 2 mA·cm^{-2}, the tensile strength decreased with an increase in the current density due to the aggregation of significant quantities of hydrogen atoms, which can lead to hydrogen damage. In addition, the tensile strength of the Nb-bearing steel decreased more slowly than that of the Nb-free steel, which is primarily because the nanosized NbC precipitates, which functioned as irreversible hydrogen traps, pinned the hydrogen atoms, causing them to be distributed around the dispersed precipitates in the matrix before the traps reached hydrogen saturation. In other words, the NbC precipitates reduced the hydrogen concentration of the matrix, hindered the accumulation of hydrogen at potential crack nucleation sites, and delayed hydrogen damage.

As expected, the total elongation of the test samples decreased significantly with an increase in the hydrogen-charging current density (Fig. 7(a)). The elongation of the Nb-bearing samples was greater than that of the Nb-free samples due to their differences in plasticity and HIC susceptibility. To further investigate the HIC susceptibility, we introduced a reduction in elongation, i.e., hydrogen-induced ductility loss. Here, the ratio of elongation reduction (I_δ) with the current density of i can be calculated using the following equation:

$$I_\delta = (1 - \delta_i/\delta_0) \times 100\% \quad (1)$$

where δ_0 and δ_i are the elongations of the test sample charged with a current density of 0 mA·cm^{-2} and of i, respectively. As shown in Fig. 7(b), elongation is further reduced (i.e., the reduction value increases) with an increase in current density. However, the ratio of elongation reduction in the Nb-bearing sample is obviously lower than that of the Nb-free sample. These results reveal that hydrogen increases the brittleness of steel, whereas the presence of Nb or NbC decreases the HIC susceptibility of steel. Moreover, as the hydrogen-charging current density was increased from 2 to 10 mA·cm^{-2}, the slope of I_δ of the Nb-bearing samples became larger than that of the Nb-free samples, which indicates that the effect of the precipitates on HIC resistance had a downward trend with an increase in the hydrogen-charging current density. We can predict that surplus hydrogen would play its expected role in HIC after hydrogen has saturated the traps induced by the precipitates.

3.3. Fracture surfaces

Fig. 8 shows the variations in the fractured surfaces of the samples at various hydrogen-charging current densities. As shown in the top views of typical fracture surfaces in the micrographs, the fracture mechanism in the test steels changed from ductile to brittle cracking with an increase in the hydrogen-charging current density.

Fig. 8(a_2) shows a micrograph of the fractured surface of a hydrogen-uncharged Nb-bearing sample after the SSRT, which exhibits the dimpled surface typical of microvoid coalescence. The fractured surface of the sample still shows ductile features (Fig. 8(b_2)) when the charging current density was 2 mA·cm^{-2}, but the dimples are shallower than those in the uncharged Nb-bearing sample, and the density is lower than that of the uncharged Nb-bearing sample. When the charging current density was 5 mA·cm^{-2}, the fractured morphology of the Nb-bearing sample differed from that charged at low current density, with a brittle intergranular fracture appearing at the outer edge while the ductility in the central region was retained, and the dimples becoming smaller and shallower with an increase in the charging current density. When the charging current density reached 10 mA·cm^{-2}, all the fractured surface of the Nb-bearing sample became brittle. These differences in morphology are due to the greater hydrogen absorption in these regions caused by the increased charging current density in the samples. As a result, diffusible hydrogen becomes available and the proportion of the brittle region is larger in the fractured surface of the charged samples.

A comparison of the magnified views of Nb-bearing and Nb-free samples shows that the ductility of the Nb-free samples is obviously poor. Fig. 8(e_2) shows that the ductile surface of the Nb-free sample has dimples that are shallower than those of the corresponding Nb-bearing sample. Fig. 8(f_2) shows a micrograph of a fractured Nb-free sample cathodically hydrogen charged with a current density of 2 mA·cm^{-2}, the surface of which is similar only to the fractured surface of the Nb-bearing sample that was cathodically charged at a current density of 5 mA·cm^{-2}. Figs. 8(g_2) and 8(h_2) show that brittle fracture occurred when the charging current was higher than 2 mA·cm^{-2}, whereby Fig. 8(h_2) with the higher hydrogen-charging current density exhibits a more brittle surface.

The main reason for the different degrees of HIC resistance between the Nb-bearing and Nb-free samples are the presence of the nanosized NbC precipitates, which function as irreversible hydrogen traps. As a result, hydrogen atoms are pinned around the precipitates and are distributed more uniformly in the matrix, which alleviates hydrogen accumulation and reduces the tendency toward hydrogen embrittlement. In addition, grain boundaries with hydrogen trap activation energies of approximately 26 kJ/mol (low-angle grain

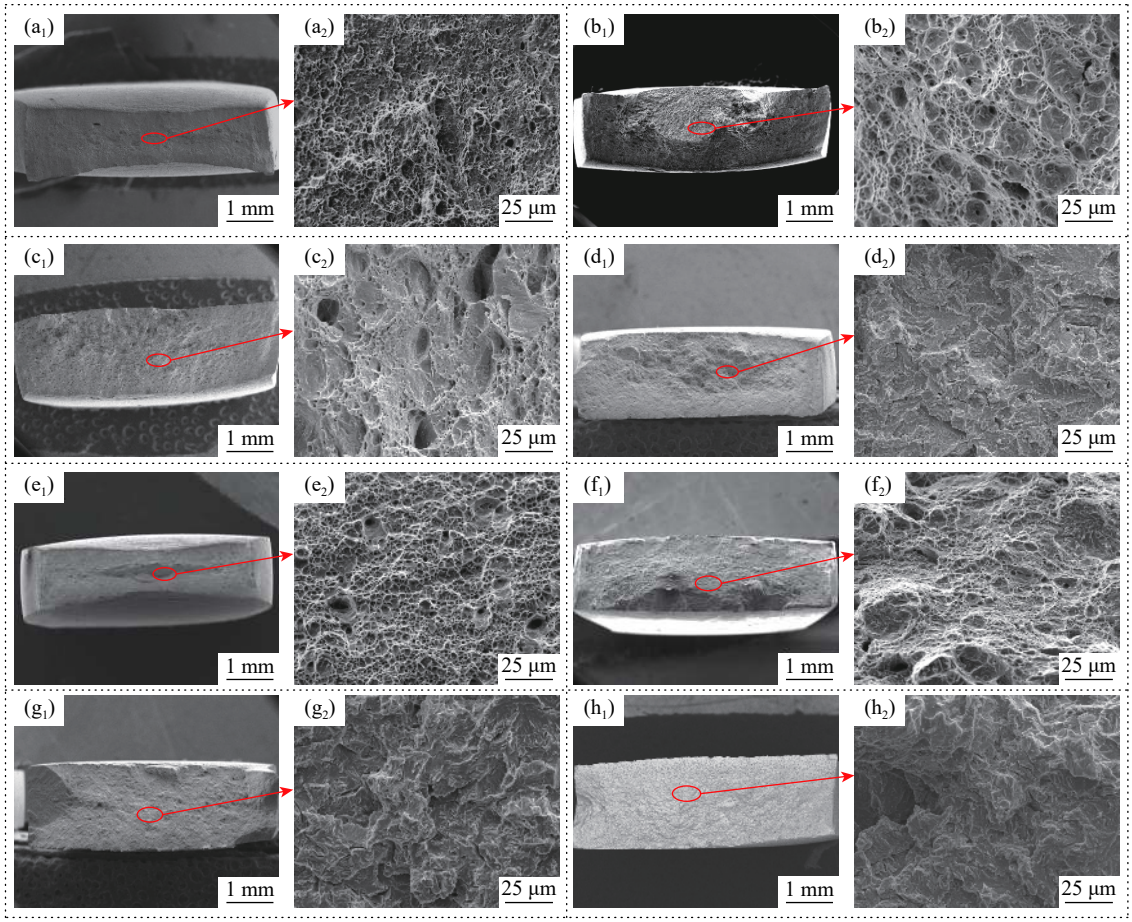

Fig. 8. Micrographs showing the top view of typical fracture surfaces at various current densities: (a_1) Nb-bearing, 0 mA·cm^{-2}; (b_1) Nb-bearing, 2 mA·cm^{-2}; (c_1) Nb-bearing, 5 mA·cm^{-2}; (d_1) Nb-bearing, 10 mA·cm^{-2}; (e_1) Nb-free, 0 mA·cm^{-2}; (f_1) Nb-free, 2 mA·cm^{-2}; (g_1) Nb-free, 5 mA·cm^{-2}; (h_1) Nb-free, 10 mA·cm^{-2}. Magnified views of fracture at various current densities: (a_2) Nb-bearing, 0 mA·cm^{-2}; (b_2) Nb-bearing, 2 mA·cm^{-2}; (c_2) Nb-bearing, 5 mA·cm^{-2}; (d_2) Nb-bearing, 10 mA·cm^{-2}; (e_2) Nb-free, 0 mA·cm^{-2}; (f_2) Nb-free, 2 mA·cm^{-2}; (g_2) Nb-free, 5 mA·cm^{-2}; (h_2) Nb-free, 10 mA·cm^{-2}.

boundary as a reversible trap) and 59 kJ/mol (high-angle grain boundary as irreversible trap) are increased via the refining grains of the nanosized NbC precipitates, which further decreases the diffusible hydrogen concentration in the matrix [4,11,33].

3.4. Effects of NbC on HIC

Hydrogen traps can be divided into two categories based on the trap activation energy in previous studies [33–34], in which the reversible traps include low-angle grain boundaries, dislocations, substitution atoms, and vacancies, while the irreversible traps include high-angle grain boundaries, precipitated second phases, inclusions, and microvoids. In fact, the types of the hydrogen traps induced by precipitates are related to the particle size and the interface coherency. The NbC precipitates with several nanometers in size form coherent interfaces with the bcc-Fe matrix, which possess the highest strain energy and acted as the effective irreversible trap for hydrogen. On the other hand, the semi-coherent interface demonstrated a weaker capacity for hydrogen trapping, and incoherent interface was further weaker to trap hydrogen [35–37]. The added Nb influences the effect of hydrogen traps in steel in two respects. First, the highly dispersed precipitates function as irreversible hydrogen traps with high activation energies. Second, nanosized NbC precipitates prevent grain growth by pinning the grain boundaries, thus, the number of grain boundaries acting as reversible hydrogen traps increase. According to previous research, for 0.055wt% Nb X80 steel, the ratio of the quantity of the hydrogen captured by reversible traps to that captured by irreversible traps was 4:9 [4,36].

The schematic in Fig. 9 shows that hydrogen atoms accumulate at the grain boundaries in steel. Hydrogen damage occurs as the local hydrogen concentration reaches a critical value. Generally, defects such as inclusions, microvoids, and dislocations absorb hydrogen atoms and determine the initial locations of HIC. In Nb-bearing steel, large quantities of NbC precipitates disperse uniformly throughout the matrix. These nanosized NbC precipitates act as irreversible traps, and uniformly pin hydrogen atoms to prevent local hydrogen accu-

mulation, which decreases the concentration of hydrogen at potential crack nucleation sites (such as the defects and interfaces) and delays HIC. Moreover, the nanosized NbC precipitates refine the grain, adding boundary interface as hydrogen traps, which further decreases the local hydrogen concentration and further inhibits HIC.

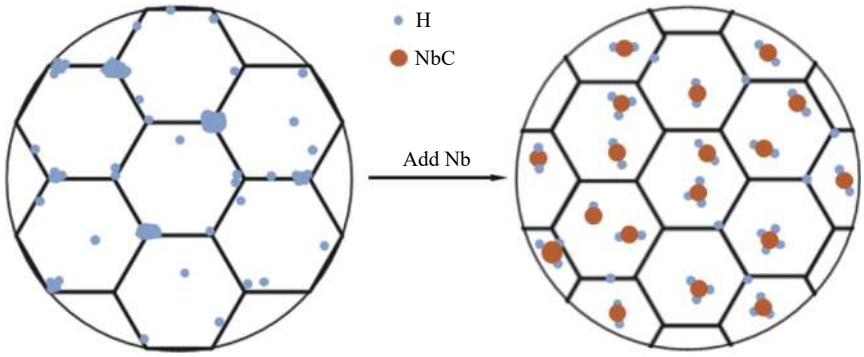

Fig. 9. Schematic illustration of the effect of NbC on HIC.

According to the above mechanism, after hydrogen has saturated the traps induced by the precipitates, the surplus hydrogen would go on to play its regular role in HIC. Nevertheless, the critical hydrogen content to induce HIC is increased by the addition of Nb to steel. That is, nanosized NbC precipitates are beneficial to the HIC resistance of HSLA steel.

4. Conclusions

(1) The HIC resistance of HSLA steel can be significantly improved by the nanosized NbC precipitates, with the main mechanism being that highly dispersed nanosized NbC precipitates act as irreversible hydrogen traps, hinder the accumulation of hydrogen at potential crack nucleation sites, and inhibit HIC.

(2) The beneficial effect of nanosized NbC precipitates on the HIC resistance of Nb-bearing HSLA steel may weaken as the irreversible traps induced by the precipitates approach hydrogen saturation.

(3) As in Nb-free steel, Nb-bearing HSLA steel presents both H-solution strengthening and the resistance to HIC, although the strength and the resistance to HIC of Nb-bearing steel are improved.

Acknowledgements

This work was financially supported by the National Key Research and Development Program of China (No. 2016YFB0300604), the National Natural Science Foundation of China (Nos. 51971033 and 51801011), the National Basic Research Program of China (No. 2014CB643300), and the National Materials Corrosion and Protection Data Center.

References

[1] D. Hardie, E.A. Charles, and A.H. Lopez, Hydrogen embrittlement of high strength pipeline steels, *Corros. Sci.*, 48(2006), No. 12, p. 4378.

[2] A.J. Haq, K. Muzaka, D.P. Dunne, A. Calka, and E.V. Pereloma, Effect of microstructure and composition on hydrogen permeation in X70 pipeline steels, *Int. J. Hydrogen Energy*, 38(2013), No. 5, p. 2544.

[3] G. Lovicu, M. Bottazzi, F. D'Aiuto, M. De Sanctis, A. Dimatteo, C. Santus, and R. Valentini, Hydrogen embrittlement of automotive advanced high-strength steels, *Metall. Mater. Trans. A*, 43(2012), No. 11, p. 4075.

[4] S.Q. Zhang, Y.H. Huang, B.T. Sun, Q.L. Liao, H.Z. Lu, B. Jian, H. Mohrbacher, W. Zhang, A.M. Guo, and Y. Zhang, Effect of Nb on hydrogen-induced delayed fracture in high strength hot stamping steels, *Mater. Sci. Eng. A*, 626(2015), p. 136.

[5] Y. Komatsuzaki, H. Joo, and K. Yamada, Influence of yield strength levels on crack growth mode in delayed fracture of structural steels, *Eng. Fract. Mech.*, 75(2008), No. 3-4, p. 551.

[6] S.Q. Zheng, Y.M. Qi, C.F. Chen, and S.Y. Li, Effect of hydrogen and inclusions on the tensile properties and fracture behavior of A350LF2 steels after exposure to wet H_2S environments, *Corros. Sci.*, 60(2012), p. 59.

[7] W. Wu, Z.Y. Liu, S.S. Hu, X.G. Li, and C.W. Du, Effect of pH and hydrogen on the stress corrosion cracking behavior of duplex stainless steel in marine atmosphere environment, *Ocean Eng.*, 146(2017), p. 311.

[8] D. Hejazi, A.J. Haq, N. Yazdipour, D.P. Dunne, A. Calka, F. Barbaro, and E.V. Pereloma, Effect of manganese content and microstructure on the susceptibility of X70 pipeline steel to hydrogen cracking, *Mater. Sci. Eng. A*, 551(2012), p. 40.

[9] L. Lin, B.S. Li, G.M. Zhu, Y.L. Kang, and R.D. Liu, Effect of niobium precipitation behavior on microstructure and hydrogen induced cracking of press hardening steel 22MnB5, *Mater. Sci. Eng. A*, 721(2018), p. 38.

[10] S.Q. Zhang, Q.Y. Zhao, J. Liu, F. Huang, Y.H. Huang, and X.G. Li, Understanding the effect of niobium on hydrogen-induced blistering in pipeline steel: A combined experimental and theoretical study, *Corros. Sci.*, 159(2019), art. No. 108142.

[11] S.Q. Zhang, E.D. Fan, J.F. Wan, J. Liu, Y.H. Huang, and X.G. Li, Effect of Nb on the hydrogen-induced cracking of high-strength low-alloy steel, *Corros. Sci.*, 139(2018), p. 83.

[12] R.J. Shi, Z.D. Wang, L.J. Qiao, and X.L. Pang, Effect of *in-situ* nanoparticles on the mechanical properties and hydrogen embrittlement of high-strength steel, *Int. J. Miner. Metall. Mater.*,

(2020). DOI: /10.1007/s12613-020-2157-2
[13] A. Nagao, M.L. Martin, M. Dadfarnia, P. Sofronis, and I.M. Robertson, The effect of nanosized (Ti,Mo)C precipitates on hydrogen embrittlement of tempered lath martensitic steel, *Acta Mater.*, 74(2014), p. 244.
[14] L.F. Li, B. Song, Z.Y. Cai, Z. Liu, and X.K. Cui, Effect of vanadium content on hydrogen diffusion behaviors and hydrogen induced ductility loss of X80 pipeline steel, *Mater. Sci. Eng. A*, 742(2019), p. 712.
[15] L. Cho, E.J. Seo, D.H. Sulistiyo, K.R. Jo, S.W. Kim, J.K. Oh, Y.R. Cho, and B.C. De Cooman, Influence of vanadium on the hydrogen embrittlement of aluminized ultra-high strength press hardening steel, *Mater. Sci. Eng. A*, 735(2018), p. 448.
[16] Q.Q. Qiao, L. Lu, E.D. Fan, J.B. Zhao, Y.L. Liu, G.C. Peng, Y.H. Huang, and X.G. Li, Effects of Nb on stress corrosion cracking of high-strength low-alloy steel in simulated seawater, *Int. J. Hydrogen Energy*, 44(2019), No. 51, p. 27962.
[17] S.Q. Zhang, J.F. Wan, Q.Y. Zhao, J. Liu, F. Huang, Y.H. Huang, and X.G. Li, Dual role of nanosized NbC precipitates in hydrogen embrittlement susceptibility of lath martensitic steel, *Corros. Sci.*, 164(2020), art. No. 108345.
[18] Z.J. Xie, X.P. Ma, C.J. Shang, X.M. Wang, and S.V. Subramanian, Nano-sized precipitation and properties of a low carbon niobium micro-alloyed bainitic steel, *Mater. Sci. Eng. A*, 641(2015), p. 37.
[19] Z.H. Wang, J.S. Wu, J. Li, X.G. Wu, Y.H. Huang, and X.G. Li, Effects of niobium on the mechanical properties and corrosion behavior of simulated weld HAZ of HSLA steel, *Metall. Mater. Trans. A*, 49(2018), p. 187.
[20] X.W. Chen, G.Y. Qiao, X.L. Han, X. Wang, F.R. Xiao, and B. Liao, Effects of Mo, Cr and Nb on microstructure and mechanical properties of heat affected zone for Nb-bearing X80 pipeline steels, *Mater. Des.*, 53(2014), p. 888.
[21] S.L. Jeng, H.T. Lee, H.Y. Huang, and R.C. Kuo, Effects of Nb on the microstructure and elevated-temperature mechanical properties of alloy 690-SUS 304L dissimilar welds, *Mater. Trans.*, 49(2008), No. 6, p. 1270.
[22] J. Takahashi, K. Kawakami, and Y. Kobayashi, Origin of hydrogen trapping site in vanadium carbide precipitation strengthening steel, *Acta Mater.*, 153(2018), p. 193.
[23] A. Turk, D. San Martín, P.E.J. Rivera-Díaz-del-Castillo, and E.I. Galindo-Nava, Correlation between vanadium carbide size and hydrogen trapping in ferritic steel, *Scripta Mater.*, 152(2018), p. 112.
[24] Z.X. Peng, J. Liu, F. Huang, Q. Hu, Z.Y. Cheng, S. Liu, and Y.F. Cheng, Effect of submicron-scale MnS inclusions on hydrogen trapping and HIC susceptibility of X70 pipeline steels, *Steel Res. Int.*, 89(2018), No. 7, art. No. 1700566.
[25] J. Ma, F. Feng, B.Q. Yu, H.F. Chen, and L.F. Fan, Effect of cooling temperature on the microstructure and corrosion behavior of X80 pipeline steel, *Int. J. Miner. Metall. Mater.*, 27(2020), No. 3, p. 347.
[26] P. Zhao, C. Cheng, G. Gao, W. Hui, R.D.K. Misra, B. Bai, and Y. Weng, The potential significance of microalloying with niobium in governing very high cycle fatigue behavior of bainite/martensite multiphase steels, *Mater. Sci. Eng. A*, 650(2016), p. 438.
[27] A.G. Kalashami, A. Kermanpur, E. Ghassemali, A. Najafizadeh, and Y. Mazaheri, Correlation of microstructure and strain hardening behavior in the ultrafine-grained Nb-bearing dual phase steels, *Mater. Sci. Eng. A*, 678(2016), p. 215.
[28] T. Zhang, J. Long, X.L. Sun, Y. Su, and Z.X. Li, Relationship between threshold stress of hydrogen induced cracking and hydrogen permeation for X80 pipeline steel, *Mater. Mech. Eng.*, 27(2003), p. 14.
[29] P.P. Bai, J. Zhou, B.W. Luo, S.Q. Zheng, P.Y. Wang, and Y. Tian, Hydrogen embrittlement of X80 pipeline steel in H2S environment: Effect of hydrogen charging time, hydrogen-trapped state and hydrogen charging releasing–recharging cycles, *Int. J. Miner. Metall. Mater.*, 27(2020), No. 1, p. 63.
[30] M.A.V. Devanathan and Z. Stachurski, The mechanism of hydrogen evolution on iron in acid solutions by determination of permeation rates, *J. Electrochem. Soc.*, 111(1964), No. 5, p. 619.
[31] R. Wang, Effects of hydrogen on fracture of pre-cracking samples of X70 pipeline steel, *J. Chin. Soc. Corros. Prot.*, 28(2008), No. 2, p. 81.
[32] G.P. Tiwari, A. Bose, J.K. Chakravartty, S.L. Wadekar, M.K. Totlani, R.N. Arya, and R.K. Fotedar, A study of internal hydrogen embrittlement of steels, *Mater. Sci. Eng. A*, 286(2000), No. 2, p. 269.
[33] G. M. Pressouyre, A classification of hydrogen traps in steel, *Metall. Trans. A*, 10(1979), No. 10, p. 1571.
[34] P. CastañoRivera, V.P. Ramunni, and P. Bruzzoni, Hydrogen trapping in an API 5L X60, *Corros. Sci.*, 54(2012), p. 106.
[35] J. Li, J.S. Wu, Z.H. Wang, S.Q. Zhang, X.G. Wu, Y.H. Huang, and X.G. Li, The effect of nanosized NbC precipitates on electrochemical corrosion behavior of high-strength low-alloy steel in 3.5%NaCl solution, *Int. J. Hydrogen Energy*, 42(2017), No. 34, p. 22175.
[36] Q.Q. Cui, J.S. Wu, D.H. Xie, X.G. Wu, Y.H. Huang, and X.G. Li, Effect of nanosized NbC precipitates on hydrogen diffusion in X80 pipeline steel, *Materials* (*Basel*), 10(2017), No. 7, p. 721.
[37] F.G. Wei, T. Hara, and K. Tsuzaki, Nano-precipitates design with hydrogen trapping character in high strengthsteels, [in] Y. Weng, H. Dong, and Y. Gan, eds., *Advanced Steels*, Springer, Berlin, Heidelberg, 2011, p. 87.